Global and Planetary Change 121 (2014) 101–112

Contents lists available at ScienceDirect

Global and Planetary Change

journal homepage: www.elsevier.com/locate/gloplacha

Reconstructed moisture evolution of the deserts in northern China since the Last Glacial Maximum and its implications for the East Asian Summer Monsoon

Qin Li [a,b,*], Haibin Wu [a], Yanyan Yu [a], Aizhi Sun [a,b], Slobodan B. Marković [c], Zhengtang Guo [a]

[a] Key Laboratory of Cenozoic Geology and Environment, Institute of Geology and Geophysics, Chinese Academy of Sciences, Beijing, 100029, China
[b] University of Chinese Academy of Sciences, Beijing, 100049, China
[c] Chair of Physical Geography, Faculty of Sciences, University of Novi Sad, Novi Sad, 21000, Serbia

ARTICLE INFO

Article history:
Received 23 January 2014
Received in revised form 9 July 2014
Accepted 15 July 2014
Available online 23 July 2014

Keywords:
East Asian summer monsoon
effective moisture
dune activity
vegetation
Last Glacial Maximum
sea level

ABSTRACT

The East Asian summer monsoon (EASM) affects rainfall variability and consequently terrestrial ecosystems in the densely populated Asian region. Understanding the nature of EASM evolution is vital for interpreting the paleoclimatic conditions of the region and for predicting future climate changes. However, the relative importance of factors such as high northern latitude ice volume, low northern latitude summer insolation and atmospheric carbon dioxide (CO_2) levels in controlling the EASM on orbital timescales remains controversial. The aeolian deposits and vegetation in the dry lands of northern China are highly sensitive to climatic changes. Here, we present a reconstruction of effective moisture levels in the region since the Last Glacial Maximum based on an analysis of changes in the sedimentary facies of aeolian deposits and vegetation type combined with reliable age control. The results demonstrate that extremely arid conditions prevailed from approximately 21-16 ka BP; that conditions gradually became wetter from 16-8 ka BP, reaching a peak in effective moisture from 8-4 ka BP; and that relatively arid conditions prevailed thereafter. This pattern of moisture evolution probably reflects changes in summer monsoon precipitation. Although the strengthening of the EASM lagged variations in northern hemisphere insolation and atmospheric CO_2 content, the strengthening was in phase with the rise in sea level from 21-6 ka BP which was controlled by changes in global ice volume. Therefore our results suggest that sea level rise may have been a major driver of EASM precipitation in the desert area of northern China during this period, as a result of shortening the transport distance of oceanic moisture sources to the continental interior and thus enabling the monsoon rainfall belt to reach the study region.

1. Introduction

The East Asian summer monsoon (EASM) is one of the major monsoon systems in the global climate system and plays a significant role in global hydrological and energy cycles (An et al., 2000). Climate model simulations (Kutzbach, 1981; COHMAP, 1988; Kutzbach and Liu, 1997; Liu et al., 2009) and paleoclimatic data (Ding et al., 1994; Liu, 1997; Wang et al., 2001; Hao et al., 2012; Lu et al., 2013) suggest that three dominant mechanisms may influence orbital-scale variations of the EASM.

First, variations in northern hemisphere ice volume have been proposed as a major factor in controlling the EASM (Liu and Ding, 1992; Ding et al., 1995; Liu, 1997; Porter, 2001). Enlarged ice-sheets in high latitudes of the northern hemisphere would cause sea-level lowering (Peltier and Fairbanks, 2006; Dutton and Lambeck, 2012), cooling of ocean surface water (Chen and Huang, 1998; Jin et al., 2012), and an intensification and southward displacement of the northern hemisphere Westerlies and the Siberian high-pressure system (Ruddiman and Kutzbach, 1989; Chen and Huang, 1998). These factors would impede the northward migration of moisture-laden monsoon airflows in northern China and thus weaken the EASM (Ding et al., 2005). This view is based on variations in the magnetic susceptibility record of aeolian dust deposits in the Chinese Loess Plateau, which co-vary significantly with global ice volume (Ding et al., 1994, 1995, 2002; Liu, 1997; Hao et al., 2012). Second, orbitally-induced changes in solar insolation are the predominant driver of the EASM (Kutzbach, 1981; COHMAP, 1988; An et al., 1990; Berger and Loutre, 1991; Morrill et al., 2003; Ruddiman, 2008). Changes in Earth's orbital parameters control low latitude insolation, thereby influencing land-ocean thermal contrasts thus leading to changes in the summer monsoon system. This view is confirmed by the $\delta^{18}O$ record of stalagmites (Wang et al., 2001, 2008; Yuan et al., 2004; Dykoski et al., 2005; Hu et al., 2008; Cheng et al., 2009). Third, atmospheric carbon dioxide (CO_2) may exert a significant influence on the EASM because an increase in CO_2 could intensify the

* Corresponding author at: Institute of Geology and Geophysics, Chinese Academy of Sciences, Beijing, 100029, China. Tel.: +86 10 82998408.
E-mail address: Liqin@mail.iggcas.ac.cn (Q. Li).

http://dx.doi.org/10.1016/j.gloplacha.2014.07.009
0921-8181/

EASM by increasing the temperature of high northern latitudes (Liu et al., 2009; Liu et al., 2012b), thus leading to a northward shift of the intertropical convergence zone (ITCZ) (Hu et al., 2000; Broccoli et al., 2006). This viewpoint is supported by the record of variations in the total organic matter content (TOC) and organic carbon isotopic composition from the Chinese Loess Plateau (Lu et al., 2013).

Contrasting views regarding the relative importance of these influences on the EASM may be the result of uncertainties in the interpretation of the proxy indices generated from various climatic archives and records (Ding et al., 2001; Herzschuh, 2006; Clemens et al., 2010; Pausata et al., 2011; Tan, 2013). However, they may also result from the fact that the EASM is a spatially complex phenomenon (An et al., 2000; Conroy and Overpeck, 2011; Jin et al., 2014) in that different regions respond differently to forcing. The ecosystem in the marginal region of the EASM in northern China is highly sensitive to past climatic changes (Lu et al., 2005; Sun et al., 2006a). Therefore, an increased number of reliable and well-dated proxy records are required to reconstruct the evolution of the EASM in the monsoon marginal region, not only to better understand the evolution of the EASM and its forcing mechanisms in this region but also to test the possibility of the occurrence of spatial differences in the response of the monsoon to various potential forcing mechanisms.

The desert in northern China, extending from the central Asian arid zone, is a key region of the mid-latitude drylands in the Asian continental interior. Most of the deserts are located in the marginal zone of the EASM, where the vegetation is highly sensitive to monsoon climate changes (Lu et al., 2005; Sun et al., 2006a; Yang and Scuderi, 2010). In addition, aeolian deposits are widely distributed in the desert and provide a record of the history of moisture changes as a result of the influence of the EASM (An, 2000; Porter, 2001). These deposits include well-sorted aeolian sand, paleosols and/or loess (Gao et al., 1993; Li et al., 2002; Lu et al., 2011; Yu and Lai, 2012), which are reliable indicators of dry, wet and moderately wet conditions, respectively (Li et al., 2002; Xiao et al., 2002; Sun et al., 2006a; Mason et al., 2009; Lu et al., 2011; Liu et al., 2012a; Yang et al., 2012).

Previous work on aeolian deposits (Dong, 2002; Li et al., 2002; Lu et al., 2005; Sun et al., 2006a; Mason et al., 2009) has successfully reconstructed the history of the humidity of several sites or of specific localities in the deserts of northern China since the Last Glacial Maximum (LGM). However, heretofore there has been no comprehensive investigation of the evolution of the humidity of entire deserts in northern China, and in addition little is known about the associated vegetation changes.

In the present study, we reconstructed the evolution of humidity in the deserts of northern China since the LGM based on analysis of the sedimentary facies of aeolian deposits and of vegetation type. The study has two novel aspects: Firstly, the reconstruction is based on a comprehensive distribution of sites, with detailed age controls of the aeolian deposits, which cover the entire desert area of northern China and, in particular the western deserts; and secondly, the quantitative biomization method was used to reconstruct the vegetation changes. Our overall objective is to characterize in detail the sequence of alternating humidity conditions and thus to improve understanding of the forcing mechanisms of the EASM in northern China.

2. Data and methods

2.1. The study region and site selection

The deserts in northern China are located in the region between 35-50°N, 75-125°E and cover an area of 1.3 million km^2 (Zhu et al., 1980). The area of sandy deserts comprises 45.3%; that of gravel deserts, 43.5%; and that of desertified lands, 11.2% (Zhu et al., 1980). Geographically, the deserts located in the arid areas west of the Helan Mountains are designated the West Desert, whereas the sandy lands distributed in the semi-arid regions east of the Helan Mountains are designated the East Sandy Land (Zhu et al., 1980) (Fig. 1).

The EASM plays a significant role in controlling the hydrologic balance and effective moisture of the East Sandy Land (Winkler and Wang, 1993; Dong et al., 1996; Lu et al., 2005), while the West Desert is mainly under the control of the northern hemisphere Westerlies (Li, 1990; Vandenberghe et al., 2006). Under the influence of the monsoon systems, the present-day annual rainfall decreases sharply from more than 400 mm in the semi-arid eastern regions to below 50 mm in the arid northwestern regions (Fig. 1), and the vegetation changes from steppe to desert steppe and to desert, in parallel with the changes in rainfall (Fig. 1).

In the last two decades, many climatic studies of aeolian deposits in deserts (Lu et al., 2005, 2011; Yang et al., 2012; Yu and Lai, 2012; Qiang et al., 2013), and of pollen assemblages from sedimentary deposits in deserts (Herzschuh et al., 2004; Jiang et al., 2006; Zhao et al., 2009a, 2009b; Sun and Feng, 2013), have been conducted. A synthesis of these records provides a useful means of reconstructing the humidity changes in the entire desert area of north China. In the present study, we analyzed records of aeolian deposits together with pollen data from all relevant publications from 1980 to 2013. The aeolian sequences were selected based on the following two criteria: (1) The whole sequence consisted entirely of aeolian deposits, so that the sedimentary facies represent a direct response to prevailing humidity conditions; and (2) an independent and reliable chronology for the aeolian sand, paleosol and/or loess was available for the post-LGM interval. The dating methods used included optically stimulated luminescence (OSL), thermoluminescence (TL), accelerator mass spectrometry (AMS) and liquid scintillation counting (LSC) ^{14}C. The pollen sites were selected based on two criteria: (1) availability of a reliable chronology with a minimum of three independent age control points; and (2) a high sampling resolution with a minimum of 200 years per sample.

Based on these criteria, a total of 115 aeolian deposit records were selected (Fig. 1 and Table S1 in the supporting information (SI)). These sections have a total of 525 age control points (69% OSL, 19% LSC ^{14}C, 6% AMS ^{14}C, 5% TL). Thirty-one pollen sequences were compiled, covering the entire desert region, and which had 234 age control points (62% AMS ^{14}C, 33% LSC ^{14}C, 4% OSL) (Fig. 1, and Table S2 in the SI). We digitized the published pollen diagrams and then recalculated the pollen percentages based on the total number of terrestrial pollen types (excluding aquatic pollen and spores from ferns and algae).

2.2. Methods

2.2.1. Chronology

The chronological data for the aeolian deposits and lake sediment sequences comprise OSL, TL, and ^{14}C dates. Some of the ^{14}C dates were in calendar years BP, while other dates were uncalibrated. In order to obtain a set of comparable chronologies for all of the records, we performed a unified calibration procedure prior to establishing the age model for each site. The ^{14}C ages were converted to calendar ages using the latest Intcal13 calibration dataset (Reimer et al., 2013).

The ages for the aeolian sand, paleosol and loess boundaries of the aeolian deposits were calculated using linear interpolation. Wherever possible we used interpolation between dates, or extrapolation of dates, within the same stratigraphic layer, rather than using dates from adjacent stratigraphic layers where there was a greater possibility of significant differences in sediment accumulation rate. If there was only a single age control point in a record, we retained that record and used the control point to age roughly to constrain the age of the sedimentary facies at that site.

The age-depth models for the pollen records from lake sediments (75%) were estimated using linear regression or interpolation. The remaining pollen records (25%) were from aeolian deposits and the construction of the age-depth models followed the procedure used for the sedimentary facies records.

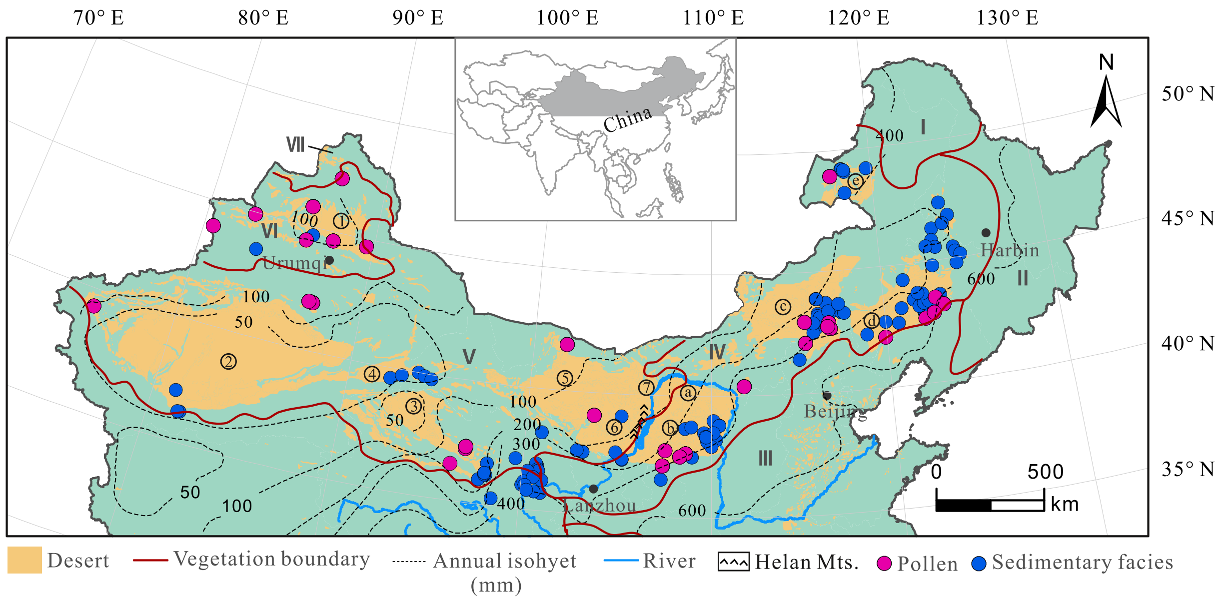

Fig. 1. Location of sedimentary facies records and fossil pollen sites in the deserts and Sandy Lands in northern China used in this study (see Table S1 and Table S2 for detailed site information). Numbers and letters in circles indicate the different Sandy Lands and deserts: 1, Gurbantunggut; 2, Taklamakan; 3, Kumtag; 4, Chaidamu; 5, Badain Jaran; 6, Tengger; 7, Wulanbuhe; a, Kubuqi; b, Maowusu; c, Otindag; d, Horqin; e, Hulunbeier. The modern distribution of vegetation types is also shown (after Zhang, 2007). Roman numerals indicate the modern vegetation zones: I Cold coniferous forest; II Cool mixed forest; III Temperate deciduous forest; IV East temperate steppe; V East temperate desert; VI Eastern desert; VII Western steppe.

2.2.2. The moisture record indicated by the sedimentary facies of aeolian deposits

The alternation of aeolian sand, paleosol and/or loess is an indicator of variations in the extent of aeolian activity and hence effective moisture (Dong et al., 1989; Dong, 2002). Within the sequence of aeolian deposits, aeolian sand represents dune-field expansion under dry conditions, whereas paleosols indicate an increase of pedogenesis under wet conditions, which leads to dune stabilization (Lu et al., 2005, 2011; Mason et al., 2009; Qiang et al., 2013). Loess is a transitional deposit which implies moderately moist conditions (Lu et al., 2006). Our methodology for reconstructing and synthesizing the moisture history of the sites was as follows.

(1) The sedimentary facies history at individual sites was determined thus: (i) A three-class ordinal wetness index for aeolian deposits, coded as '1' (aeolian sand), '2' (loess) or '3' (paleosol), was used to represent dry, moderately wet and wet conditions, respectively. (ii) Based on the estimated ages of the boundaries between aeolian sand, paleosol or loess, the sedimentary facies history was obtained for each individual site. (iii) The sedimentary facies history was determined for each 500-year time interval at each individual site.
(2) Based on the sedimentary facies history of 115 aeolian deposits, we reconstructed the record of temporal moisture evolution for the desert of northern China. This was achieved by calculating the percentages of aeolian sand, loess, and paleosol records for each 500-year time interval. An increased percentage of paleosols indicates increased humidity, while an increased percentage of aeolian sand indicates decreased humidity. In order to detect possible differences between the moisture evolution of the East Sandy Land and the West Desert, we performed separate calculations of the percentages of aeolian sand, loess and paleosol records for each region (Fig. 3a, b).
(3) Finally, the spatial pattern of moisture evolution of the deserts was reconstructed using ArcGIS software to plot the codes representing the different deposit types at a 1000-year interval (Fig. 2 and Fig. S1 in the SI).

2.2.3. Moisture variations indicated by biome type

In arid, semi-arid and semi-humid regions, vegetation is very sensitive to moisture conditions (Editorial Board for Natural Geography of China, 1995; An et al., 2000; Zhao et al., 2009a). For example, a significant precipitation gradient exists in northern China from >600 mm in the semi-humid eastern regions to <50 mm in the arid northwestern regions, and the vegetation changes correspondingly from wooded grassland to meadow steppe to desert steppe and then to desert (Zhang, 2007).

In the present study, vegetation type was quantitatively reconstructed using the biomization method, which was developed in Europe (Prentice et al., 1996) and has subsequently been tested successfully and applied in several other regions including Africa, Japan, Soviet Union, Eurasia and North America (Williams et al., 1998; Yu et al., 1998; Allen et al., 2000; Gotanda et al., 2002; Tarasov et al., 2007). The vegetation and the associated moisture history were reconstructed as follows.

(1) The vegetation evolution at individual sites was reconstructed thus: (i) On the basis of the constructed age model and the recalculated sequence of pollen percentages after digitization, time series of pollen percentages were constructed. (ii) We resampled each of the original time series at a 1000-year interval by averaging the original data in each time window. (iii) The vegetation was reconstructed using the biomization method using the classification of plant functional types (PFTs) and biome assignment in China (Members of China Quaternary Pollen Data, 2001), and was performed using the 3P-base software (Guiot and Goeury, 1996). (iv) Finally, the vegetation type at a 1000-year time interval was reconstructed for each site.
(2) The temporal moisture history indicated by the vegetation composition was determined thus: Based on the vegetation reconstructions for 31 sites, we calculated the percentages of each vegetation type in each time interval at all the pollen sites. Changes in vegetation composition can indicate relative changes in moisture conditions. For example, increased percentages of desert-type vegetation indicate a shift to drier conditions, while

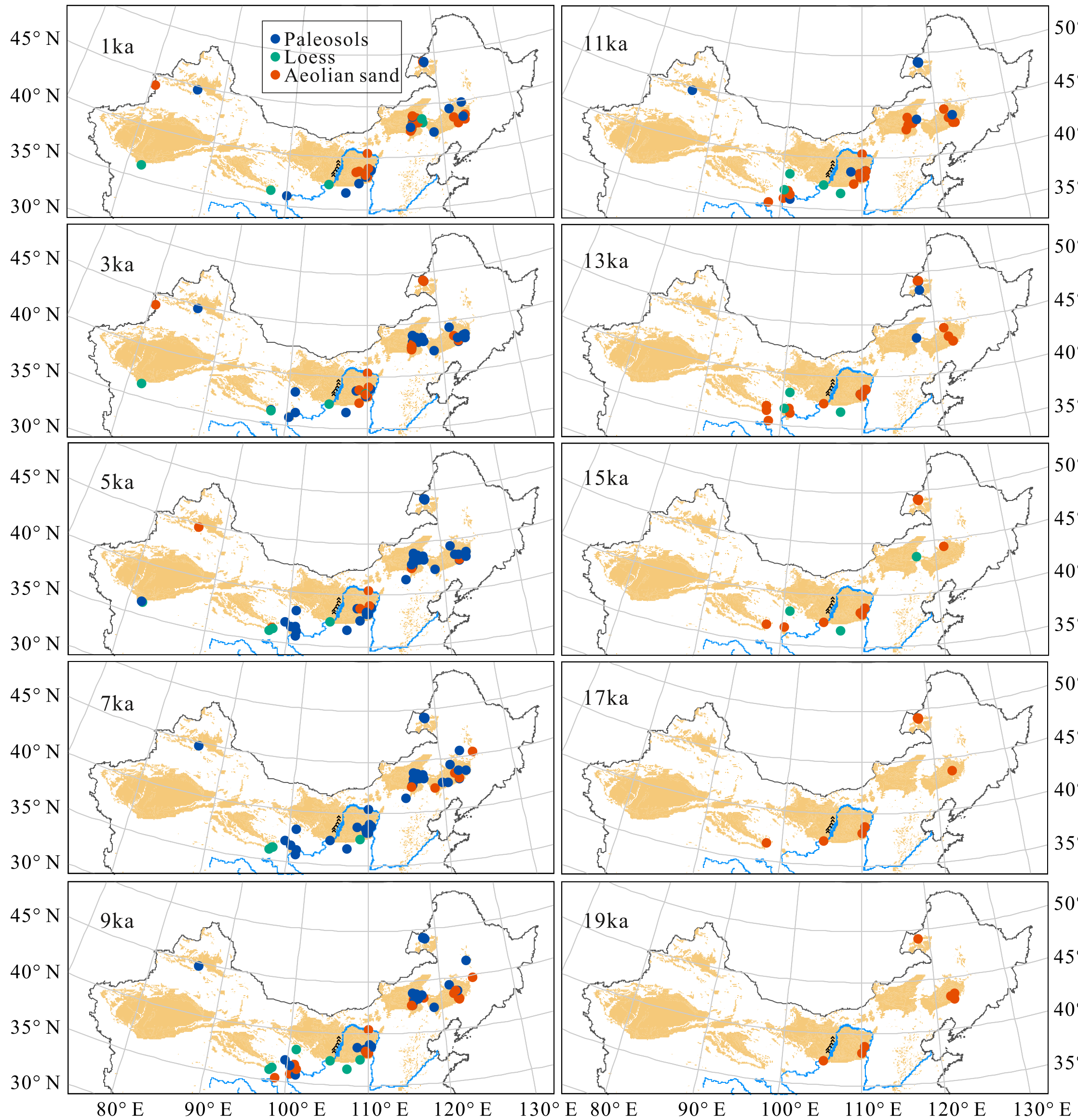

Fig. 2. Spatial patterns of sedimentary facies evolution in the deserts of northern China in 1000-year intervals since the LGM.

an increase in the steppe or forest-steppe percentage implies a shift to moister conditions. Because the vegetation types were significantly different between the East Sandy Land (including desert (DESE), steppe (STEP), cool mixed forest (COMX), and temperate deciduous forest (TEDE)) and the West Desert (only including DESE and STEP) since the LGM, we calculated the vegetation percentages for the two regions separately (Fig. 3c, d).

(3) The spatial pattern of moisture changes since the LGM, as indicated by the vegetation reconstructions, was represented using ArcGIS software (Fig. 4 and Fig. S2 in the SI).

3. Results

Figs. 2–4 illustrate the temporal and spatial patterns of moisture evolution since the LGM based on sedimentary facies and vegetation type. The principal features are summarized as follows:

Stage 1 (21-16 ka BP) - The deserts in both the East Sandy Land and the West Desert were characterized by aeolian sand (Fig. 2, Fig. S1 in the SI and Fig. 3a, b) and were occupied by DESE vegetation (Fig. 4, Fig. S2 in the SI and Fig. 3c, d), indicating the occurrence of extremely arid conditions in northern China during at this time.

Stage 2 (16 to 8 ka BP) - The aeolian sand retreated (Fig. 2 and Fig. S1 in the SI), which is consistent with the increased percentages of loess and paleosol (Fig. 3a, b). STEP occurred in the East Sandy Land (Fig. 3c, 4, and Fig. S2 in the SI), and in the West Desert STEP appeared in the surrounding desert areas (Fig. 4 and Fig. S2 in the SI), with a slight increase in the STEP percentage (Fig. 3d). These changes in sedimentary facies and vegetation type indicate a gradual increase in humidity in both regions.

Stage 3 (8-4 ka BP) - Palaeosol development was widespread (Fig. 2 and Fig. S1 in the SI), and the maximum percentage (Fig. 3a) since the LGM occurred in the East Sandy Land. The STEP type extended into the deserts, and in addition several forest types (including COMX and TEDE) were located in the southern margin of the Otindag and Horqin Sandy Land (Fig. 4 and Fig. S2 in the SI). Although paleosol and loess records were limited in the West Desert and in addition exhibited a particularly scattered distribution on

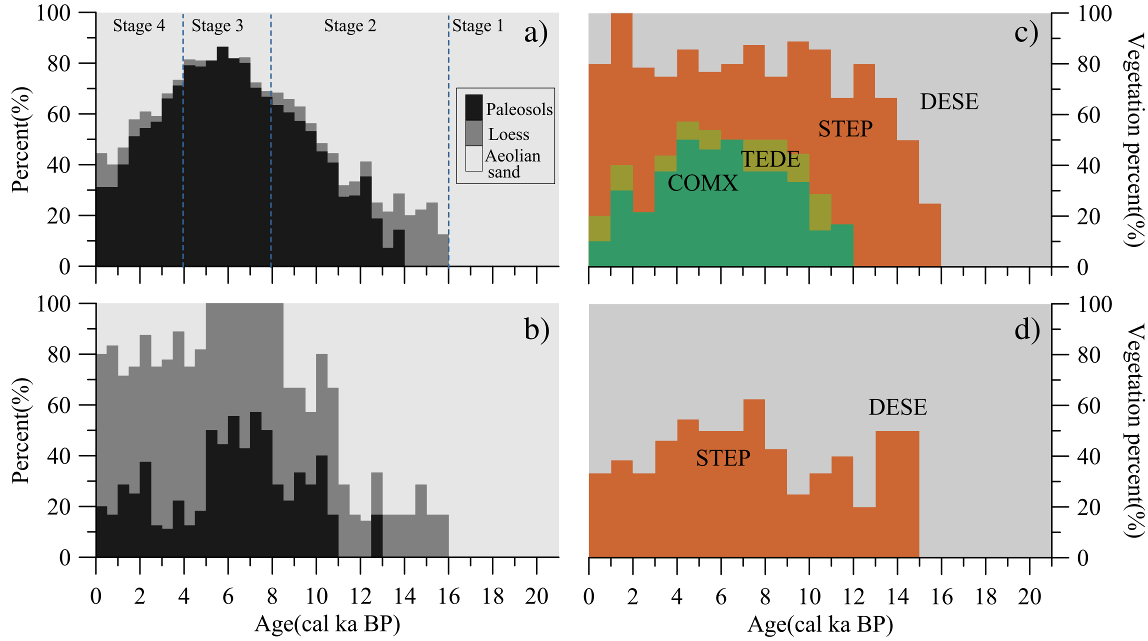

Fig. 3. Temporal changes of sedimentary facies (sand/loess/paleosol) and vegetation type since the LGM. Percentage changes in the aeolian units of the study sites in (a) the East Sandy Land (the evolution of moisture was divided into four stages: stage 1, 21-16 ka BP; stage 2, 16-8 ka BP; stage 3, 8-4 ka BP; stage 4, 4-0 ka BP.) and (b) the West Desert. Percentage changes in the vegetation type of the study sites in (c) the East Sandy land and (d) the West Desert. The vegetation types are: COMX, cool mixed forest; TEDE, temperate deciduous forest; DESE, desert; STEP, steppe.

the margins of the Kumtag, Gurbantunggut and Taklamakan deserts (Fig. 2), the percentages of paleosol and loess (Fig. 3b) demonstrate a increased trend and a maximum. Meanwhile the percentages of STEP type increased slightly (Fig. 3d), although the vegetation was still dominated by DESE type in the West Desert (Fig. 2). This maximum percentage occurrence of palaeosol and loess in both desert regions is coincident with a peak in either the steppe or forest vegetation type, suggesting that effective moisture in the deserts was at its highest level during the mid-Holocene period.

Stage 4 (after 4 ka BP) - The percentages of paleosol and loess decreased (Fig. 2, Fig. S1 in the SI, and Fig. 3a, b), and the steppe and forest types retreated to the southern margin of the East Sandy Land (Fig. 4 and Fig. S2 in the SI). In the West Desert, the percentage of desert also increased (Fig. 3d and 4 and Fig. S2 in the SI). These results suggest that the climate in northern China became arid during the late Holocene.

4. Discussion

4.1. Comparison with previous records for moisture evolution

The comparison illustrated in Fig. 5 demonstrates that our moisture curve (Fig. 5a) for the East Sandy land based on sedimentary facies agrees well with records from regions adjacent to the deserts, including tree pollen percentages in the eastern Tibetan Plateau (Fig. 5b, Zhao et al., 2011); a combination of tree pollen percentages, pollen concentration, the *Artemisia*-to-Chenopodiaceae ratio, and percentages of *Ephedra* and *Nitraria* in the northwestern Loess Plateau and eastern Inner Mongolia (Fig. 5b, Zhao et al., 2009a); tree and shrub pollen percentages in the semi-arid belt in northern China (Fig. 5c, Wang and Feng, 2013); and the tree pollen percentages (Fig. 5d) in the monsoon marginal region of northern China including Hani peat (Yu et al., 2008), Bayanchagan (Jiang et al., 2006) and Daihai (Xiao et al., 2002). Our results are also consistent with the magnetic susceptibility record of the Loess Plateau (Fig. 5e, Peterse et al., 2011), which is widely used to indicate changes in monsoon precipitation (An et al., 1991; Liu and Liu, 1991). All of these records confirm that humidity, as indicated by sedimentary facies and vegetation type, generally increased from the LGM to the mid-Holocene, reached a maximum during the mid-Holocene (~8-4 ka BP), and then decreased in the late Holocene. The timing of the interval of maximum moisture values (Fig. 5b) varies between the different proxies, which may be attributed to differences in their climatic responses.

The observed pattern of moisture variability also agrees with the results of previous studies based on analysis of the sedimentary facies of aeolian deposits in the East Sandy Land (Li et al., 2002; Lu et al., 2006; Sun et al., 2006a; Mason et al., 2009; Yang and Scuderi, 2010; Yang et al., 2012). However, a significant difference between the present study and previous work is that our reconstruction of moisture history combines changes in sedimentary facies and in vegetation type. We consider that the use of vegetation type imparts an increased robustness to our reconstruction since vegetation is an excellent indicator of moisture conditions (Herzschuh et al., 2004; Jiang et al., 2006; Zhao et al., 2009b). Furthermore, our data set contains a significant number of additional records (115 aeolian deposit sites) based on data published from 1980 to 2013, and in addition we have expanded the focus of previous studies on the East Sandy Land to include the West Desert. Therefore, our reconstruction spans the entire desert region in northern China.

It is noteworthy that pollen records (Zhao et al., 2009a), geomorphological, lacustrine, pedological and geochemical records (Yang et al., 2011), together with both a synthesis of multi-proxy records and climate model simulations (Jin et al., 2014) for northwestern China dominated by the Westerlies, also indicate that effective moisture gradually increased in the early Holocene, reached a peak in the mid-Holocene (8.5 to 4-5.5 ka BP), and then declined in the late Holocene. This finding is generally consistent with our results obtained by combining records of sedimentary facies and vegetation type in the West Desert.

4.2. Moisture evolution and its implications for EASM precipitation in the desert areas of northern China

Effective moisture is calculated as precipitation (P) minus potential evapotranspiration (PE) (Roads et al., 1994; Peterson et al., 2002).

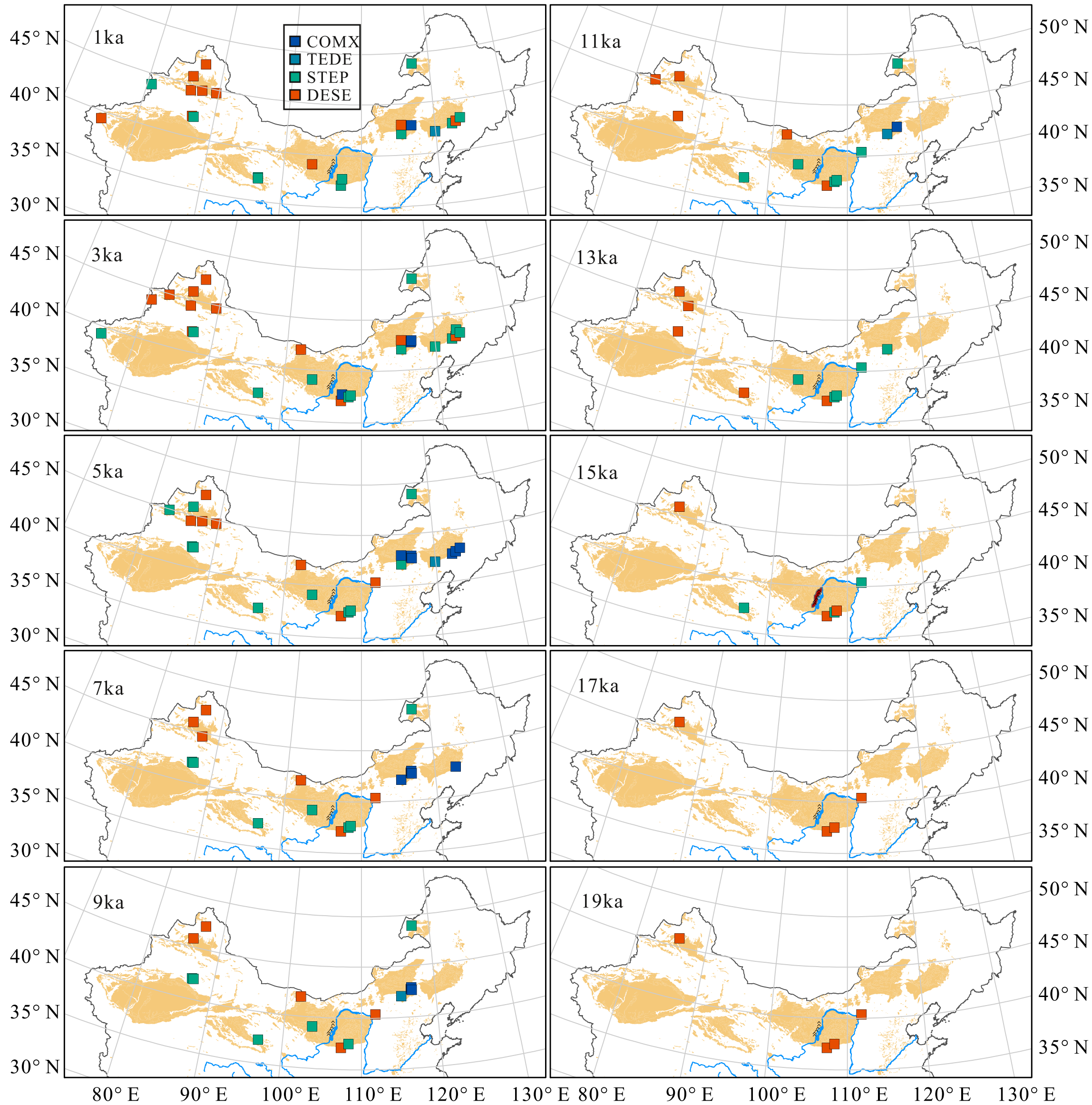

Fig. 4. Spatial patterns of vegetation evolution in the deserts of northern China in 1000-year intervals since the LGM. The vegetation types are: COMX, cool mixed forest; TEDE, temperate deciduous forest; DESE, desert; STEP, steppe.

Because PE is controlled by temperature (Monteith, 1965), it is possible to infer changes in precipitation based on variations in effective moisture and temperature. Because we did not reconstruct temperature in the deserts, their temperature history was estimated via comparison with data from the adjacent Loess Plateau. These data are based on the MBT/CBT paleothermometer (Peterse et al., 2011). Although clearly site-specific temperature data for the deserts would be preferable, the temperature variations on the Loess Plateau are in good agreement with a stacked temperature reconstruction (Fig. 6a) from 30-90°N and global records (Shakun et al., 2012; Marcott et al., 2013) based on various types of paleotemperature proxy (e.g., alkenones, Mg/Ca ratios in planktonic foraminifera, and fossil pollen), indicating that since the LGM local temperature variations in the region were generally consistent with global temperature changes. This suggests that it is acceptable to use the temperature record of the Loess Plateau to estimate temperature trends in the desert, although the absolute temperature values of the Loess Plateau and the desert may differ due to local environmental contrasts.

From 21 to 16 ka BP, the moisture level was extremely low (Fig. 6h). In addition to the weak evapotranspiration indicated by the low temperatures (Fig. 6a), this result suggests that monsoon precipitation was also low. From 16 to 8 ka BP, the moisture level increased (Fig. 6h), accompanied by an increase in temperature (Fig. 6a). Because higher temperatures would have strengthened evapotranspiration, this suggests that monsoon precipitation increased during this period. From 8 to 4 ka BP, the moisture levels reached maximum values (Fig. 6h) with the highest temperature (maximum evaporation) since the LGM, which indicates that monsoon precipitation was at a maximum. During the late Holocene, moisture declined with decreasing temperature (lower evapotranspiration), indicating that monsoon precipitation was decreasing. In summary, our results suggest that the EASM precipitation was at a very low level from 21 to 16 ka BP; it then began to increase gradually from 16 to 8 ka BP, before reaching its peak from 8-4 ka BP, and then declined after 4 ka BP.

These inferred changes in the EASM in the desert areas of northern China differ from those in southern China based on the $\delta^{18}O$ record of stalagmites (Wang et al., 2001, 2008; Yuan et al., 2004; Dykoski et al., 2005). The latter indicates that monsoon intensity followed the summer insolation trend of the northern hemisphere, with the maximum monsoon intensity occurring in the early Holocene and decreasing thereafter

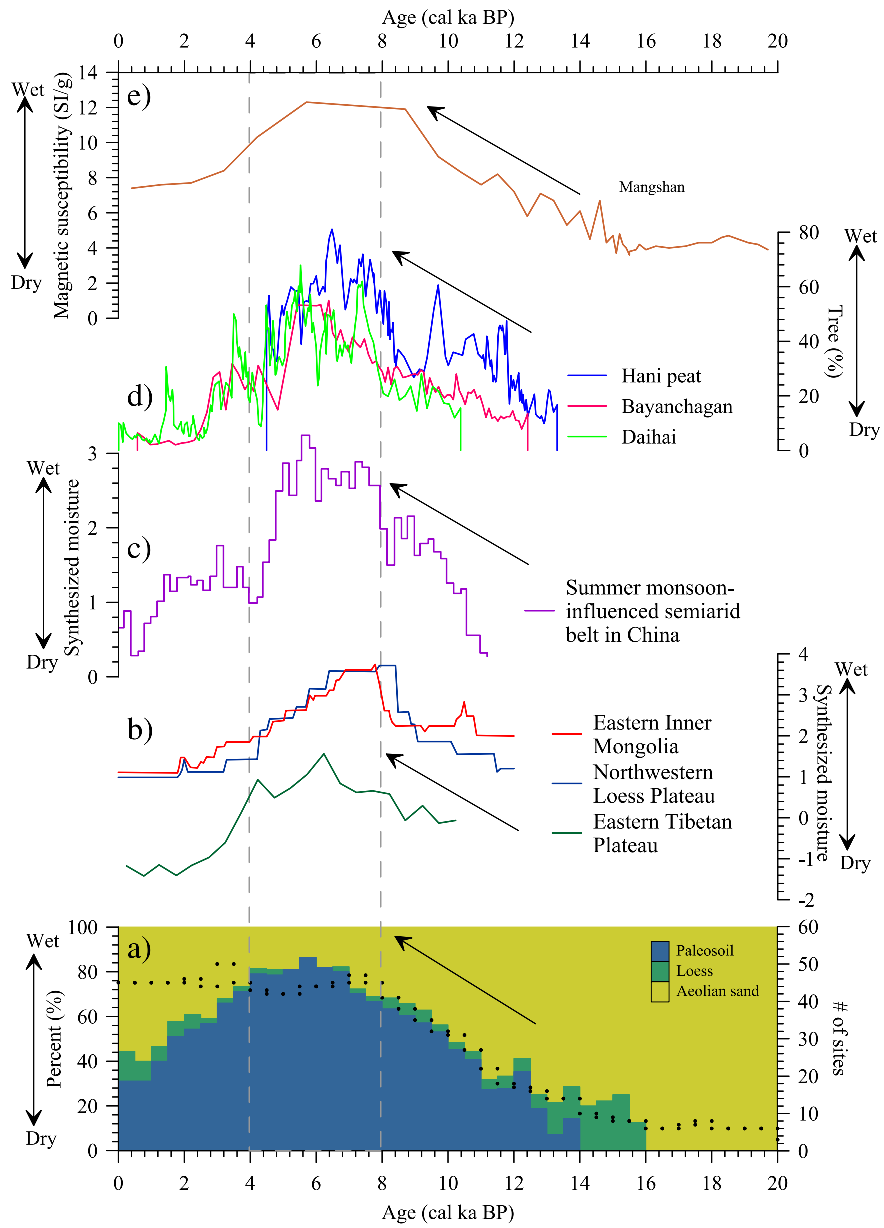

Fig. 5. Comparison of the effective moisture levels indicated by sedimentary facies in the East Sandy Land (scatter point- # of sites) (a) with the following proxy moisture records: (b) a synthesized moisture record based on pollen proxies (percentages of tree or tree and shrub pollen, percentages of *Ephedra* and *Nitraria* pollen and ratios of *Artemisia*-to-Chenopodiaceae pollen) in the northwestern Loess Plateau, eastern Inner Mongolia, and Eastern Tibetan Plateau (Zhao et al., 2009a; 2011); (c) a moisture record based mainly on the percentages of trees and shrubs in the semi-arid belt in northern China (Wang and Feng, 2013); (d) tree pollen percentages in the Hani peat (Yu et al., 2008), Bayanchagan (Jiang et al., 2006) and Daihai (Xiao et al., 2002); and (e) the magnetic susceptibility record at Mangshan in the Chinese Loess Plateau (Peterse et al., 2011).

(Kutzbach, 1981; COHMAP, 1988). The difference may be ascribed partly to the different proxes used, and partly to the spatial complexity of the monsoon (An et al., 2000; Conroy and Overpeck, 2011; Jin et al., 2014). In addition, our reconstruction of the moisture history of the West Desert differs somewhat to that of Chen et al., (2008) for arid central Asia. The latter indicates that the climate was dry during the early Holocene while in contrast in our study effective moisture levels gradually increased at that time; however, both studies indicate that the moisture optimum occurred in the mid-Holocene. Again, the difference may result from the different climate proxies used: for example, Chen et al., (2008) used a moisture index based on a comprehensive reconstruction of lake levels using $\delta^{18}O$, $\delta^{13}C$, $CaCO_3$, grain size, and pollen data from lake sediments. In contrast, our use of sedimentary facies and vegetation type constitutes a consistent methodology which was applied uniformly to all of our study sites.

4.3. Possible forcing mechanisms of EASM evolution in the desert area of northern China

Three main factors have been invoked to explain changes in the EASM during glacial-interglacial cycles: firstly, Earth orbitally-induced changes in solar insolation (Kutzbach, 1981; COHMAP, 1988; An et al., 1990; Berger and Loutre, 1991); secondly, atmospheric CO_2 concentration (Kripalani et al., 2007; Liu et al., 2009; Lu et al., 2013); and thirdly, changes in Arctic ice-sheets (Liu and Ding, 1992; Ding et al., 1995, 2005; Liu, 1997; Porter, 2001). A comparison of our reconstructed EASM

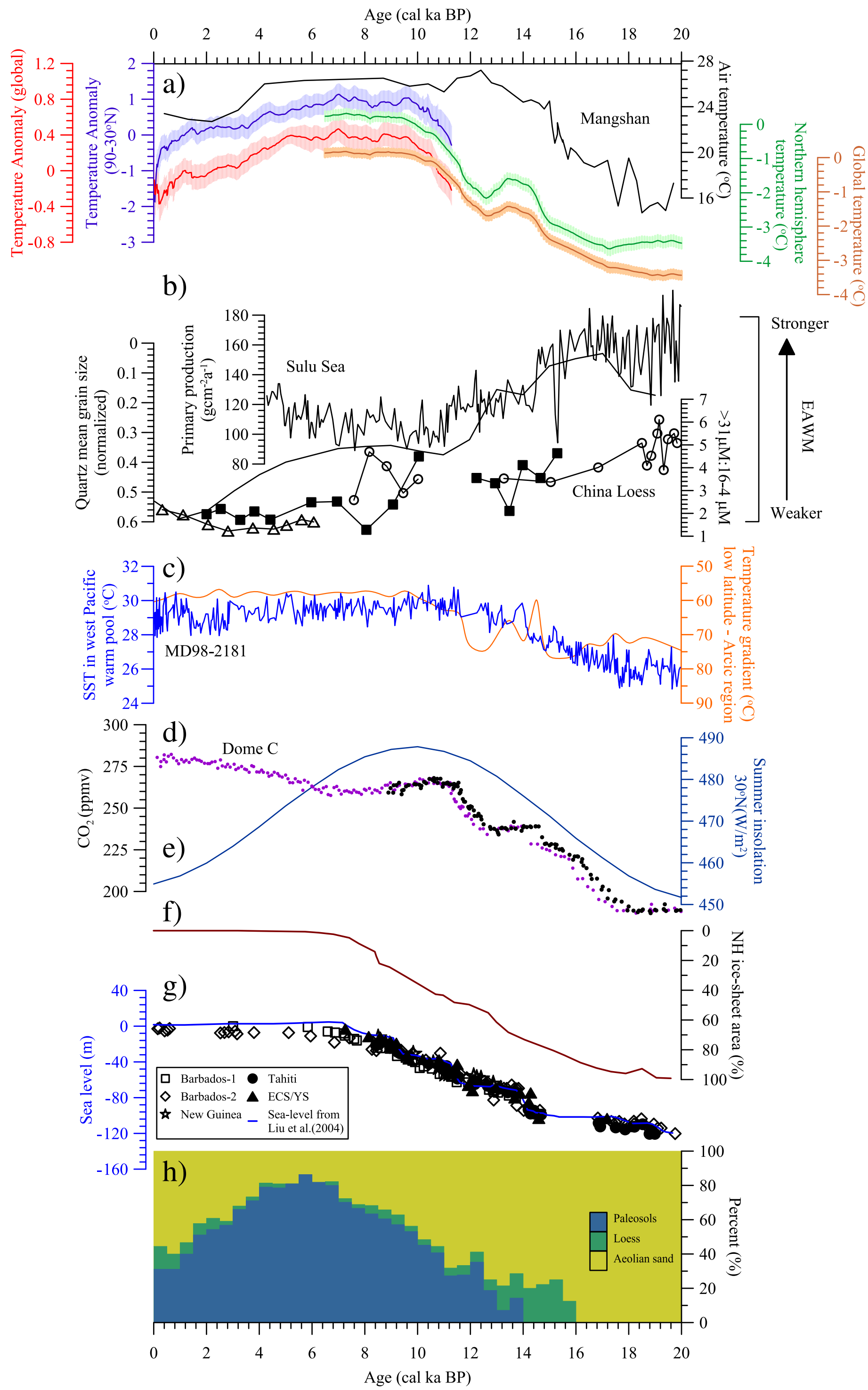

Fig. 6. Comparison of effective moisture levels based on the history of aeolian activity with other paleoclimatic records. (a) Temperature changes at Mangshan in the Chinese Loess Plateau (Peterse et al., 2011) (the black line), the mean temperature from 30-90°N, and global temperature (Shakun et al., 2012; Marcott et al., 2013). (b) Proxy records of EAWM intensity from the primary productivity of the Sulu Sea (de Garidel-Thoron et al., 2001), normalized mean quartz grain size record of Chinese loess (Sun et al., 2006b, 2006c), and bulk grain size records of Chinese loess (Stevens et al., 2007). (c) Temperature gradient between the low latitude and Arctic regions expressed as the low latitude average temperature minus the Arctic average temperature (orange line, the Fig S3, S4 in the SI represents the data processing steps); the Arctic temperature records from NGRIP and GRIP (Rasmussen et al., 2006, 2008; Andersen et al., 2006 - Fig. S4a in SI); and 17 low latitude temperature records from the northern hemisphere tropical ocean (Shakun et al., 2012 - Fig. S4b in SI). Sea surface temperature (SST) of core MD98-2181 in the western Pacific warm pool (blue line, Stott et al., 2007). (d) Atmospheric carbon dioxide (CO_2) concentration from Dome Concordia, Antarctica (Lüthi et al., 2008 - purple dots; Parrenin et al., 2013 - black dots). (e) Summer (JJA) insolation at 30°N (Berger and Loutre, 1991). (f) Northern Hemisphere ice-sheet area derived from summing the extents of the Laurentide, Cordilleran and Scandinavian ice sheets (Dyke, 2004). (g) Sea level changes based on coral reef data, peat and shallow marine deposits (Bard et al., 1990, 1996; Fairbanks, 1990; Edwards et al., 1993; Siddall et al., 2003; Liu et al., 2004). (h) History of effective moisture in the present study based on the sedimentary facies of the East Sandy land in northern China.

precipitation record with solar insolation reveals that our record (Fig. 6h) significantly lags (by approximately 4 ka) changes in low latitude (30°N) northern hemisphere summer insolation (Fig. 6e). Similar lags have been reported for other records, such as total organic matter content (TOC) of loess sections, the $\delta^{13}C$ of both TOC and specific n-alkanes from the Loess Plateau (~4-5 ka lag) (Lu et al., 2013), and the pollen record of the eastern Tibetan Plateau (~4-5 ka lag) (Zhao et al., 2011). If insolation were the sole driver of the EASM, the monsoon strength would have increased gradually, in parallel with summer insolation over the LGM, to a maximum at 10 ka (Liu et al., 2014), with minimal time lag. Similarly, our monsoon precipitation record also exhibits a lag of approximately 4 ka relative to the record of atmospheric CO_2 concentration from Antarctic ice cores (Fig. 6d) (Lüthi et al., 2008; Parrenin et al., 2013). These discrepancies lead us to hypothesize that other mechanisms, and not northern hemisphere insolation or CO_2 alone, drive EASM precipitation.

Variations in EASM intensity reconstructed in our study (Fig. 6h) correlate well with variations in northern hemisphere ice volume (Fig. 6f), which suggests that this may have been a major factor in controlling monsoon evolution in the desert of northern China. Northern hemisphere ice volume affects the EASM via three main processes (Liu and Ding, 1992; Kutzbach et al., 1993; Wang, 1999; Ding et al., 2005). Firstly, the enlarged ice-sheets in high latitudes of the northern hemisphere greatly intensified the Siberian High (Kutzbach et al., 1993; Ruddiman, 2008), resulting in the intensification of the East Asian Winter Monsoon (EAWM) and the weakening of the EASM (Ding et al., 1994; Chen and Huang, 1998). In addition, the expansion of ice sheets would lead to strengthened temperature and atmospheric pressure gradients between the polar regions and the mid-low latitudes, thereby impeding the northward movement of moisture-laden monsoon airflows in northern China and hence to a weakened EASM (Liu and Ding, 1992; Ding et al., 1995; Liu, 1997; Ding et al., 2005). Secondly, the expansion of polar ice sheets would cool the low-latitude oceans, thereby reducing the evaporation of ocean water and weakening the EASM (Chen and Huang, 1998; Ruddiman, 2003; Jin et al., 2012). Thirdly, ice accumulation on continents would result in a lowering of sea-level, which would increase the distance to oceanic moisture sources again resulting in a weakening of the EASM (Liu, 1997; Wang, 1999).

We compared variations in EASM precipitation since the LGM recorded in our study with those of various proxies of potentially significant drivers: The Siberian High indicated by the EAWM (de Garidel-Thoron et al., 2001; Sun et al., 2006b, 2006c; Stevens et al., 2007; Fig. 6b) (Ding et al., 1995; Gong and Ho, 2002); temperature gradients between low latitudes (reflected by records of Mg/Ca ratio, Uk'37, TEX86) and Arctic regions (reflected by the $\delta^{18}O$ of ice cores) (the orange line in Fig. 6c, Fig. S3 and S4 in SI); sea surface temperature (SST) records in the western Pacific warm pool reconstructed from Mg/Ca ratios (the blue line in Fig. 6c); and sea level (Fig. 6g) (based on coral reef data, and data from peat deposits and shallow marine deposits). The results indicate that EASM precipitation (Fig. 6h) was correlated with increasing sea level (Fig. 6g) from 21 to 6 ka BP, with the EASM maximum coincident with the highest sea level at approximately 6 ka BP (Fig. 6g). In contrast, there is a clear discrepancy between the variation of EASM precipitation in the East Sandy Land and the intensity of the Siberian High (Fig. 6b), temperature gradients (orange line in Fig. 6c) and SST records in the western Pacific warm pool (blue line in Fig. 6c); the latter three records did not achieve peak values until the early Holocene.

The inter-relationships outlined above indicate that rising sea level rise may have been an important forcing factor for the intensification of EASM precipitation from 21 to 6 ka BP. This explanation is also supported by the strengthening of monsoon precipitation observed in Indonesia since the LGM (Griffiths et al., 2009), which was caused by the rising sea level of the Sunda Shelf from 11 to 7 ka BP. This is explained by the fact that the East Asian continental shelf forms part of the shallow continental shelf area of the western Pacific (Wang, 2004), and thus the shelf is rapidly flooded as global sea level rises. The ~120 m global sea-level rise since the LGM (Wang, 1992) would significantly reduce the distance for moisture transport from the ocean to the Asian interior (Fig. 7), with the magnitude of the transgression reaching a maximum of ~1000 km (Wang, 1992). The resulting intensification of the EASM would facilitate the northwards migration of the monsoon rainfall belt towards the inland desert.

The changes in humidity after ~4 ka BP, reflecting the weakening of the EASM, are in agreement with the co-eval decrease in northern hemisphere summer insolation, suggesting that this became an important driver of EASM precipitation in northern China once sea level reached

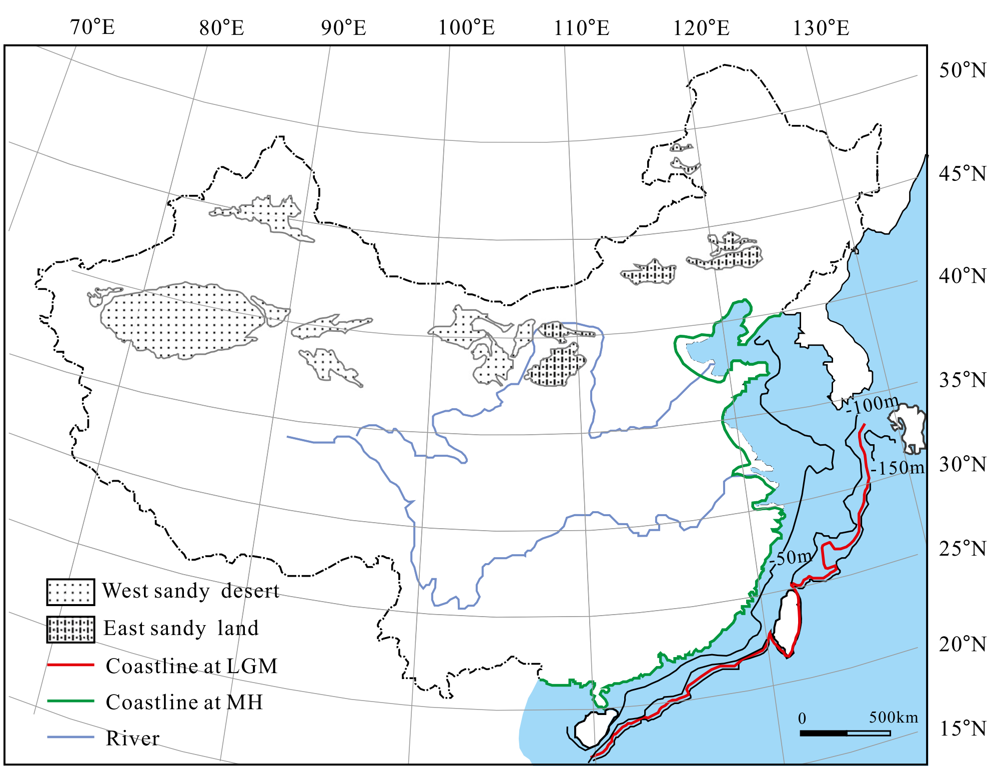

Fig. 7. Changes in the location of the coastline in China since the LGM. The paleocoastline was approximately 120 m lower during the LGM relative to the modern location (Wang, 1992), and the location of the coastline during the mid-Holocene was approximately 3-5 m higher than it is today (Zhao and Zhang, 1984; Han et al., 1992; Zhao et al., 1996).

its modern level. However, it should be noted that further research is needed in order to assess the significance of human activity in affecting the fidelity of the monsoon proxies since it is clear that this factor is likely to have significantly impacted the environment of northern China in the late Holocene (Jing, 1991; Dong et al., 1993; Rhode et al., 2007; Schlüetz and Lehmkuhl, 2009), and in particular may have disturbed both the sedimentary facies and the vegetation in the desert regions.

Our study demonstrated that the moisture history of the West Desert was similar to the East Sandy Land since the LGM. Climate change in the West Desert was under the control of the northern hemisphere Westerlies (Li, 1990), and the evolution of the humidity of the region was mainly related to SST in the North Atlantic (Chen et al., 2008; Li et al., 2011). Because the variation of North Atlantic SSTs (e.g., Kaplan and Wolfe, 2006) was similar to that of the EASM in the East Sandy Land, the history of humidity since the LGM was consistent between the West Desert and the East Sandy Land.

5. Conclusions

We have combined 115 records of the types of sedimentary facies of aeolian deposits with 31 vegetation records in order to reconstruct the history of effective moisture in the deserts of northern China since the LGM. The results demonstrate that extremely arid conditions obtained from approximately 21-16 ka BP; that the environment gradually became wetter from 16-8 kaBP with effective moisture reaching a peak from 8-4 ka BP; and that relatively arid conditions prevailed thereafter. These trends are likely to reflect changes in summer monsoon precipitation, which was highly consistent with sea level rise from 21-6 ka BP. Thus we suggest that ice volume - controlled sea level rise may have been an important driver of the EASM from 21-6 ka BP, as a result of the shortening of the moisture transport distance from the ocean to the continental interior and causing the monsoon rainfall belt to migrate northwards towards the inland desert. However, other factors, such as variations in solar insolation and atmospheric CO_2 content, may also have played an important role in the evolution of the EASM since the LGM.

Acknowledgements

This research was funded by the National Natural Science Foundation of China (Grant nos. 41071055 and 41125011), the Bairen Programs of the Chinese Academy of Sciences, the Strategic Priority Research Program (XDA05120702) and the National Basic Research Program of China (973 Program, Grant no. 2010CB950204).

Appendix A. Supplementary data

Supplementary data to this article can be found online at http://dx.doi.org/10.1016/j.gloplacha.2014.07.009.

References

Allen, J.R.M., Watts, W.A., Huntley, B., 2000. Weichselian palynostratigraphy, palaeovegetation and palaeoenvironment; the record from Lago Grande di Monticchio, southern Italy. Quat. Int. 73–74, 91–110.

An, Z.S., Xiao, J.L., Zhang, J.Z., 1990. Monsoon and climate change in the Chinese loess plateau since 130,000 years. In: Liu, T.S. (Ed.), Loess. Quaternary geology. Global change (part two). Science Press, Beijing, pp. 108–114.

An, Z.S., Wu, X.H., Wang, P.X., Wang, S.M., Dong, G.R., Sun, X.J., Zhang, D.E., Lu, Y.C., Zheng, S.H., Zhao, S.L., 1991. The evolution in China paleomonsoon since130ka:II. Paleomonsoon changes. Sci. China Ser. B 11, 1209–1215 (in chinese).

An, Z.S., 2000. The history and variability of the East Asian paleomonsoon climate. Quat. Sci. Rev. 19, 171–187.

An, Z.S., Porter, S.C., Kutzbach, J.E., Wu, X.H., Wang, S.M., Liu, X.D., Li, X.Q., Zhou, W.J., 2000. Asynchronous Holocene optimum of the East Asian monsoon. Quat. Sci. Rev. 19 (8), 743–762.

Andersen, K.K., et al., 2006. The Greenland ice core chronology 2005, 15–42ka. Part 1: constructing the time scale. Quat. Sci. Rev 25, 3246–3257.

Bard, E., Hamelin, B., Arnold, M., Montaggioni, L., Cabioch, G., Faure, G., Rougerie, F., 1996. Deglacial sea-level record from Tahiti corals and the timing of global meltwater discharge. Nature 382, 241–244.

Bard, E., Hamelin, B., Fairbanks, R.G., Zindler, A., 1990. Calibration Of The C-14 Timescale Over The Past 30,000 Years Using Mass-Spectrometric U-Th Ages From Barbados Corals. Nature 345, 405–410.

Berger, A., Loutre, M.F., 1991. Insolation values for the climate of the last 10 million years. Quat. Sci. Rev. 10, 297–317.

Broccoli, A.J., Dahl, K.A., Stouffer, R.J., 2006. Response of the ITCZ to Northern Hemisphere cooling. Geophys. Res. Lett. 33, L01702. http://dx.doi.org/10.1029/2005GL024546.

Chen, F.H., Yu, Z.C., Yang, M.L., Ito, E., Wang, S.M., Madsen, D.B., Huang, X.Z., Zhao, Y., Sato, T., Briks, H.J.B., et al., 2008. Holocene moisture evolution in arid central Asia and its out-of-phase relationship with Asian monsoon history. Quat. Sci. Rev. 27, 351–364.

Chen, M.T., Huang, C.Y., 1998. Ice-volume forcing of winter monsoon climate in the South China Sea. Paleoceanography 13, 622–633.

Cheng, H., Edwards, R.L., Broecker, W.S., Denton, G.H., Kong, X.G., Wang, Y.J., Zhang, R., Wang, X.F., 2009. Ice Age Terminations. Science 326, 248–252.

Clemens, S.C., Prell, W.L., Sun, Y.B., 2010. Orbital-scale timing and mechanisms driving Late Pleistocene Indo-Asian summer monsoons: Reinterpreting cave speleothem delta O-18. Paleoceanography 25, PA4207. http://dx.doi.org/10.1029/2010PA001926.

COHMAP, 1988. Climatic changes of the last 18,000 years: Observations and model simulations. Science 241, 1043–1052.

Conroy, J.L., Overpeck, J.T., 2011. Regionalization of Present-Day Precipitation in the Greater Monsoon Region of Asia. J. Clim. 24, 4073–4095.

De Garidel-Thoron, T., Beaufort, L., Linsley, B.K., Dannenmann, S., 2001. Millennial-scale dynamics of the East Asian winter monsoon during the last 200,000 years. Paleoceanography 16, 491–502.

Ding, Z.L., Yu, Z.W., Rutter, N.W., Liu, T.S., 1994. Towards an orbital time-scale for chinese loess deposits. Quat. Sci. Rev. 13, 39–70.

Ding, Z.L., Liu, T.S., Rutter, N.W., Yu, Z.W., Guo, Z.T., Zhu, R.X., 1995. Ice-volume forcing of east-asian winter monsoon variations in the past 800,000 years. Quat. Res. 44, 149–159.

Ding, Z.L., Yang, S.L., Sun, J.M., Liu, T.S., 2001. Iron geochemistry of loess and red clay deposits in the Chinese Loess Plateau and implications for long-term Asian monsoon evolution in the last 7.0 Ma. Earth Planet Sc. Lett. 185, 99–109.

Ding, Z.L., Derbyshire, E., Yang, S.L., Yu, Z.W., Xiong, S.F., Liu, T.S., 2002. Stacked 2.6-Ma grain size record from the Chinese loess based on five sections and correlation with the deep-sea delta O-18 record. Paleoceanography 17, 5-1–5-21.

Ding, Z.L., Derbyshire, E., Yang, S.L., Sun, J.M., Liu, T.S., 2005. Stepwise expansion of desert environment across northern China in the past 3.5 Ma and implications for monsoon evolution. Earth Planet Sc. Lett. 237, 45–55.

Dong, G.R., 2002. The evolution of the sandy desert and sandy land since late period of the last glaciation. In: Wang, S.W., Dong, G.R. (Eds.), Environmental Characters and their Evolution in the Western China. Science Press, Beijing, pp. 108–112.

Dong, G.R., Gao, S.Y., Jin, J., Li, B.S., 1989. The formation, evolution and cause of the mu-us desert in china. Sci. China Ser. B. 32, 859–872.

Dong, G.R., Gao, S.Y., Jin, J., 1993. Desertification and Controls in the Gonghe Basin. Qinghai Province. Science Press, Beijing, pp. 1–166 (in Chinese with English abstract).

Dong, G.R., Wang, G.Y., Li, X.Z., Chen, H.Z., Jin, J., 1996. The change in paleomonsoon in eastern part of China deserts since last interglacial. Sci. China Ser. D. 26, 437–444 (in Chinese).

Dutton, A., Lambeck, K., 2012. Ice volume and sea level during the last interglacial. Science 337, 216–219.

Dyke, A.S., 2004. An outline of North American deglaciation with emphasis on central and northern Canada. Quaternary Glaciations: Extent and Chronology 2, 373–424.

Dykoski, C.A., Edwards, R.L., Cheng, H., Yuan, D.X., Cai, Y.J., Zhang, M.L., Lin, Y.S., Qing, J.M., An, Z.S., Revenaugh, J., 2005. A high-resolution, absolute-dated Holocene and deglacial Asian monsoon record from Dongge Cave. China Earth Planet Sc. Lett. 233, 71–86.

Edwards, R.L., Beck, J.W., Burr, G.S., Donahue, D.J., Chappell, J.M.A., Bloom, A.L., Druffel, E.R.M., Taylor, F.W., 1993. A large drop in atmospheric C-14/C-12 and reduced melting in the younger dryas, documented with th-230 ages of corals. Science 260, 962–968.

Editorial Board for Flora of China, 1995. Flora of ChinaSciences Press, Beijing (in Chinese).

Fairbanks, R.G., 1990. The age and origin of the "younger dryas climate event" in greenland ice cores. Paleoceanography 5, 937–948.

Gao, S.Y., Chen, W.N., Jin, H.L., Dong, G.R., Li, B.S., Yang, G.S., Lin, L.Y., Guan, Y.Z., Sun, Z., Jin, J., Zhang, Y.T., Cao, J.S., 1993. Preliminary study on the Holocene evolution of the NW desert margin in the monsoon region of China. Sci. China Ser. B. 23, 202–208 (in Chinese).

Gong, D.-Y., Ho, C.-H., 2002. The Siberian High and climate change over middle to high latitude Asia. Theor. Appl. Climatol. 72, 1–9.

Gotanda, K., Nakagawa, T., Tarasov, P., Kitagawa, J., Inoue, Y., Yasuda, Y., 2002. Biome classification from Japanese pollen data: application to modern-day and late Quaternary samples. Quat. Sci. Rev. 21, 647–657.

Griffiths, M.L., Drysdale, R.N., Gagan, M.K., Zhao, J.X., Ayliffe, L.K., Hellstrom, J.C., Hantoro, W.S., Frisia, S., Feng, Y.X., Cartwright, I., Pierre, E.S., Fischer, M.J., Suwargadi, B.W., 2009. Increasing Australian-Indonesian monsoon rainfall linked to early Holocene sea-level rise. Nat. Geosci. 2, 636–639.

Guiot, J., Goeury, C., 1996. PPPBASE, a software for statistical analysis of paleoecological and paleoclimatological data. Dendrochronologia 14, 295–300.

Han, Y.S., Meng, G.L., Wang, S.Q., Zhuang, Z.Y., Xv, W.D., Xv, J.S., 1992. The mid-Holocene warm optimum and high sea-level in coastal regions of North China. In: Shi, Y.F. (Ed.), Holocene optimum climates and environments in China. China Ocean Press, Beijing, pp. 121–130.

Hao, Q.Z., Wang, L., Oldfield, F., Peng, S.Z., Qin, L., Song, Y., Xu, B., Qiao, Y.S., Bloemendal, J., Guo, Z.T., 2012. Delayed build-up of Arctic ice sheets during 400,000-year minima in insolation variability. Nature 490, 393–396.
Herzschuh, U., 2006. Palaeo-moisture evolution in monsoonal Central Asia during the last 50,000 years. Quat. Sci. Rev. 25, 163–178.
Herzschuh, U., Tarasov, P., Wunnemann, B., Hartmann, K., 2004. Holocene vegetation and climate of the Alashan Plateau, NW China, reconstructed from pollen data. Palaeogeogr. Palaeocl. 211, 1–17.
Hu, C.Y., Henderson, G.M., Huang, J.H., Xie, S., Sun, Y., Johnson, K.R., 2008. Quantification of Holocene Asian monsoon rainfall from spatially separated cave records. Earth Planet Sc. Lett. 266, 221–232.
Hu, Z.Z., Latif, M., Roeckner, E., Bengtsson, L., 2000. Intensified Asian summer monsoon and its variability in a coupled model forced by increasing greenhouse gas concentrations. Geophys. Res. Lett. 27, 2681–2684.
Jiang, W.Y., Guo, Z.T., Sun, X.J., Wu, H.B., Chu, G.Q., Yuan, B.Y., Hatte, C., Guiot, J., 2006. Reconstruction of climate and vegetation changes of Lake Bayanchagan (Inner Mongolia): Holocene variability of the East Asian monsoon. Quat. Res. 65, 411–420.
Jin, L.Y., Chen, F.H., Morrill, C., Otto-Bliesner, B.L., Rosenbloom, N., 2012. Causes of early Holocene desertification in arid central Asia. Clim. Dyn. 38, 1577–1591.
Jin, L.Y., Schneider, B., Par, W., Latif, M., Khon, V., Zhang, X.J., 2014. The spatial-temporal patterns of Asian summer monsoon precipitation in response to Holocene insolation change: a model-data synthesis. Quat. Sci. Rev. 85, 47–62.
Jing, A., 1991. Preface of the Archeological research of the desertification in Horqin desert. Chin. J. Hist. Geogr. 1, 179–183 (in Chinese).
Kaplan, M.R., Wolfe, A.P., 2006. Spatial and temporal variability of Holocene temperature in the North Atlantic region. Quat. Res. 65 (2), 223–231.
Kripalani, R.H., Oh, J.H., Chaudhari, H.S., 2007. Response of the East Asian summer monsoon to doubled atmospheric CO_2: Coupled climate model simulations and projections under IPCC AR4. Theor. Appl. Climatol. 87, 1–28.
Kutzbach, J.E., 1981. Monsoon climate of the early Holocene: climate experiment with the earth's orbital parameters for 9000 years ago. Science 214, 59–61.
Kutzbach, J.E., Guetter, P.J., Behling, P., Selin, R., 1993. Simulated climatic changes: results of the COHMAP climate-model experiments. In: Wright, H.E., et al. (Eds.), Global climates since the last glacial maximum. Univ. of Minn. Press, Minneapolis, pp. 24–93.
Kutzbach, J.E., Liu, Z., 1997. Response of the African monsoon to orbital forcing and ocean feedbacks in the middle Holocene. Science 278, 440–443.
Li, J.J., 1990. The patterns of environmental changes since late pleistocene in northwestern China. Quat. Sci. 3, 197–204 (in Chinese with English abstract).
Li, S.H., Sun, J.M., Zhao, H., 2002. Optical dating of dune sands in the northeastern deserts of China. Palaeogeogr. Palaeocl. 181, 419–429.
Li, X.Q., Zhao, K.L., Dodson, J., Zhou, X.Y., 2011. Moisture dynamics in central Asia for the last 15 kyr: new evidence from Yili Valley, Xinjiang, NW China. Quat. Sci. Rev. 30, 3457–3466.
Liu, J.P., Milliman, J.D., Gao, S., Cheng, P., 2004. Holocene development of the Yellow River's subaqueous delta, North Yellow Sea. Mar. Geol. 209, 45–67.
Liu, T.S., Ding, Z.L., 1992. Stepwise coupling of monsoon circulation to continental ice-volume variations during the past 2500,000 years. Quat. Sci. 1, 12–23 (in Chinese).
Liu, T.S., 1997. Quaternary environments. Science Press, Beijing, pp. 221–239.
Liu, X.J., Lai, Z.P., Yu, L.P., Sun, Y.J., Madsen, D., 2012a. Luminescence chronology of aeolian deposits from the Qinghai Lake area in the Northeastern Qinghai-Tibetan Plateau and its palaeoenvironmental implications. Quat. Geochronol. 10, 37–43.
Liu, X.M., Liu, T.S., 1991. Chinese loess magnetic particle analysis and paleoclimatic significance. Sci. China Ser. B. 6, 639–644 (in Chinese).
Liu, Z.Y., Otto-Bliesner, B.L., He, F., Brady, E.C., Tomas, R., Clark, P.U., Carlson, A.E., Lynch-Stieglitz, J., Curry, W., Brook, E., Erickson, D., Jacob, R., Kutzbach, J., Cheng, J., 2009. Transient Simulation of Last Deglaciation with a New Mechanism for Bolling-Allerod Warming. Science 325, 310–314.
Liu, Z.Y., Carlson, A.E., He, F., Brady, E.C., Otto-Bliesner, B.L., Briegleb, B.P., Wehrenberg, M., Clark, P.U., Wu, S., Cheng, J., Zhang, J.X., Noone, D., Zhu, J., 2012b. Younger Dryas cooling and the Greenland climate response to CO_2. PNAS 109, 11101–11104.
Liu, Z.Y., Wen, X.Y., Brady, E.C., Otto-Bliesner, B., Yu, G., Lu, H.Y., Cheng, H., Wang, Y.J., Zhang, W.P., Ding, Y.H., Edwards, R.L., Cheng, J., Liu, W., Yang, H., 2014. Chinese cave records and the East Asia Summer Monsoon. Quat. Sci. Rev. 83, 115–128.
Lu, H.Y., Miao, X.D., Zhou, Y.L., Mason, J.A., Swinehart, J., Zhang, J.F., Zhou, L.P., Yi, S.W., 2005. Late Quaternary aeolian activity in the Mu Us and Otindag dune fields (north China) and lagged response to insolation forcing. Geophys. Res. Lett. 32. http://dx.doi.org/10.1029/2005GL024560 L21716.
Lu, H.Y., Zhou, Y.L., Mason, J., Stevens, T., Yi, S.W., Swinehart, J., 2006. Late Quaternary climatic changes in Northern China——New evidences from sand dune and loess records based on optically stimulated luminescence dating. Quat. Sci. 26, 888–894 (in Chinese with English abstract).
Lu, H.Y., Zhao, C.F., Mason, J., Yi, S.W., Zhao, H., Zhou, Y.L., Ji, J.F., Swinehart, J., Wang, C.M., 2011. Holocene climatic changes revealed by aeolian deposits from the Qinghai Lake area (northeastern Qinghai-Tibetan Plateau) and possible forcing mechanisms. The Holocene 21, 297–304.
Lu, H.Y., Yi, S.W., Liu, Z.Y., Mason, J.A., Jiang, D.B., Cheng, J., Stevens, T., Xu, Z.W., Zhang, E.L., Jin, L.Y., Zhang, Z.H., Guo, Z.T., Wang, Y., Otto-Bliesner, B., 2013. Variation of East Asian monsoon precipitation during the past 21 ky and potential CO_2 forcing. Geology 41, 1023–1026.
Lüthi, D., et al., 2008. High-resolution carbon dioxide concentration record 650,000–800,000 years before present. Nature 453, 379–382.
Marcott, S.A., Shakun, J.D., Clark, P.U., Mix, A.C., 2013. A Reconstruction of Regional and Global Temperature for the Past 11,300 Years. Science 339, 1198–1201.
Mason, J.A., Lu, H.Y., Zhou, Y.L., Miao, X.D., Swinehart, J.B., Liu, Z.Y., Goble, R.J., Yi, S.W., 2009. Dune mobility and aridity at the desert margin of northern China at a time of peak monsoon strength. Geology 37, 947–950.
Members of China Quternary Pollen Data Base, 2001. Simulation of China biome reconstruction based on pollen data from surface sediment samples. Acta Bot. Sin. 43, 201–209 [in Chinese with English abstract].
Monteith, J.L., 1965. Evaporation and environment. Symp. Soc. Exp. Biol. 19, 205–234.
Morrill, C., Overpeck, J.T., Cole, J.E., 2003. A synthesis of abrupt changes in the Asian summer monsoon since the last deglaciation. The Holocene 13, 465–476.
Parrenin, F., et al., 2013. Synchronous change of atmospheric CO_2 and Antarctic temperature during the last deglacial warming. Science 339, 1060–1063.
Pausata, F.S.R., Battisti, D.S., Nisancioglu, K.H., Bitz, C.M., 2011. Chinese stalagmite delta $^{O}18$ controlled by changes in the Indian monsoon during a simulated Heinrich event. Nat. Geosci. 4, 474–480.
Peltier, W.R., Fairbanks, R.G., 2006. Global glacial ice volume and Last Glacial Maximum duration from an extended Barbados sea level record. Quat. Sci. Rev. 25, 3322–3337.
Peterse, F., Prins, M.A., Beets, C.J., Troelstra, S.R., Zheng, H.B., Gu, Z.Y., Schouten, S., Damste, J.S.S., 2011. Decoupled warming and monsoon precipitation in East Asia over the last deglaciation. Earth Planet Sc. Lett. 301, 256–264.
Peterson, B.J., Holmes, R.M., McClelland, J.W., Vorosmarty, C.J., Lammers, R.B., Shiklomanov, A.I., Shiklomanov, I.A., Rahmstorf, S., 2002. Increasing river discharge to the Arctic Ocean. Science 298, 2171–2173.
Porter, S.C., 2001. Chinese loess record of monsoon climate during the last glacial–interglacial cycle. Earth-Sci. Rev. 54, 115–128.
Prentice, C., Guiot, J., Huntley, B., Jolly, D., Cheddadi, R., 1996. Reconstructing biomes from palaeoecological data: a general method and its application to European pollen data at 0 and 6 ka. Clim. Dyn. 12, 185–194.
Qiang, M.R., Chen, F.H., Song, L., Liu, X.X., Li, M.Z., Wang, Q., 2013. Late Quaternary aeolian activity in Gonghe Basin, northeastern Qinghai-Tibetan Plateau, China. Quat. Res. 79, 403–412.
Rasmussen, S.O., et al., 2006. A new Greenland ice core chronology for the last glacial termination. J. Geophys. Res. Atmos. 1984–2012, 111 (D6).
Rasmussen, S.O., et al., 2008. Synchronization of the NGRIP, GRIP, and GISP2 ice cores across MIS 2 and palaeoclimatic implications. Quat. Sci. Rev. 27, 18–28.
Reimer, P.J., et al., 2013. IntCal13 and Marine13 radiocarbon age calibration curves 0––50,000 years cal BP. Radiocarbon 55, 1869–1887.
Rhode, D., Zhang, H., Madsen, D.B., Xing, G., Brantingham, R.J., Ma, H., Olsen, J.W., 2007. Epipaleolithic/early Neolithic settlements at Qinghai Lake, western China. J. Archaeol. Sci. 34, 600–612.
Roads, J.O., Chen, S., Guetter, A.K., Georgakakos, K.P., 1994. Large-scale aspects of the united-states hydrologic-cycle. Bull. Am. Meteorol. Soc. 75, 1589–1610.
Ruddiman, W.F., 2003. Orbital insolation, ice volume, and greenhouse gases. Quat. Sci. Rev. 22, 1597–1629.
Ruddiman, W.F., 2008. Earth's Climate Past and Future, Second Edition. W.H. Freeman and Company, New York, pp. 138–142.
Ruddiman, W., Kutzbach, J., 1989. Forcing of late Cenozoic Northern Hemisphere climate by plateau uplift in southern Asia and the American west. J. Geophys. Res.: Atmos. (1984–2012) 94 (D15), 18409–18427.
Schlüetz, F., Lehmkuhl, F., 2009. Holocene climatic change and the nomadic Anthropocene in Eastern Tibet: palynological and geomorphological results from the Nianbaoyeze Mountains. Quat. Sci. Rev. 28, 1449–1471.
Shakun, J.D., et al., 2012. Global warming preceded by increasing carbon dioxide concentrations during the last deglaciation. Nature 484, 49–54.
Siddall, M., Rohling, E.J., Almogi-Labin, A., Hemleben, C., Meischner, D., Schmelzer, I., Smeed, D.A., 2003. Sea-level fluctuations during the last glacial cycle. Nature 423, 853–858.
Stevens, T., Thomas, D.S., Armitage, S.J., Lunn, H.R., Lu, H., 2007. Reinterpreting climate proxy records from late Quaternary Chinese loess: a detailed OSL investigation. Earth-Sci. Rev. 80, 111–136.
Stott, L., Timmermann, A., Thunell, R., 2007. Southern hemisphere and deep-sea warming led deglacial atmospheric CO_2 rise and tropical warming. Science 318, 435–438.
Sun, A.Z., Feng, Z.D., 2013. Holocene climatic reconstructions from the fossil pollen record at Qigai Nuur in the southern Mongolian Plateau. The Holocene 23, 1391–1402.
Sun, J.M., Li, S.H., Han, P., Chen, Y.Y., 2006a. Holocene environmental changes in the central Inner Mongolia, based on single-aliquot-quartz optical dating and multi-proxy study of dune sands. Palaeogeogr. Palaeocl. 233, 51–62.
Sun, Y., Chen, J., Clemens, S.C., Liu, Q., Ji, J., Tada, R., 2006b. East Asian monsoon variability over the last seven glacial cycles recorded by a loess sequence from the northwestern Chinese Loess Plateau. Geochem. Geophys. Geosyst. 7. http://dx.doi.org/10.1029/2006GC001287.
Sun, Y., Clemens, S.C., An, Z., Yu, Z., 2006c. Astronomical timescale and palaeoclimatic implications of stacked 3.6-Myr monsoon records from the Chinese Loess Plateau. Quat. Sci. Rev. 25, 33–48.
Tan, M., 2013. Circulation effect: response of precipitation δ18O to the ENSO cycle in monsoon regions of China. Clim. Dyn. 1–11. http://dx.doi.org/10.1007/s00382-013-1732-x.
Tarasov, P., Bezrukova, E., Karabanov, E., Nakagawa, T., Wagner, M., Kulagina, N., Letunova, P., Abzaeva, A., Granoszewski, W., Riedel, F., 2007. Vegetation and climate dynamics during the Holocene and Eemian interglacials derived from Lake Baikal pollen records. Palaeogeogr. Palaeocl. 252, 440–457.
Vandenberghe, J., Renssen, H., van Huissteden, K., Nugteren, G., Konert, M., Lu, H.Y., Dodonov, A., Buylaert, J.P., 2006. Penetration of Atlantic westerly winds into Central and East Asia. Quat. Sci. Rev. 25, 2380–2389.
Wang, P.X., 1992. A comparative on paleoceanographic study at the marginal seas of western Pacific during last glacial. In: Ye, Z.Z., Wang, P.X. (Eds.), Contributions to Late Quaternary Paleoceanography of the South China Sea. Qingdao Ocean Univ. Press, Qingdao, pp. 308–321 (in Chinese).
Wang, P.X., 1999. Response of Western Pacific marginal seas to glacial cycles: paleoceanographic and sedimentological features. Mar. Geol. 156, 5–39.
Wang, P.X., 2004. Cenozoic deformation and the history of sea–land interactions in Asia. In: Clift, P., Wang, P.X., Kuhnt, W., Hayes, D. (Eds.), Continent–Ocean Interactions

within East Asian Marginal Seas. Geophysical Monograph 149. American Geophysical Union, Washington, DC, pp. 1–22.
Wang, W., Feng, Z.D., 2013. Holocene moisture evolution across the Mongolian Plateau and its surrounding areas: A synthesis of climatic records. Earth-Sci. Rev. 122, 38–57.
Wang, Y.J., Cheng, H., Edwards, R.L., An, Z.S., Wu, J.Y., Shen, C.C., Dorale, J.A., 2001. A high-resolution absolute-dated Late Pleistocene monsoon record from Hulu Cave, China. Science 294, 2345–2348.
Wang, Y.J., Cheng, H., Edwards, R.L., Kong, X.G., Shao, X.H., Chen, S.T., Wu, J.Y., Jiang, X.Y., Wang, X.F., An, Z.S., 2008. Millennial- and orbital-scale changes in the East Asian monsoon over the past 224,000 years. Nature 451, 1090–1093.
Williams, J.W., Summers, R.L., Webb, T., 1998. Applying plant functional types to construct biome maps from eastern North American pollen data: Comparisons with model results. Quat. Sci. Rev. 17, 607–627.
Winkler, M.G., Wang, P.K., 1993. The late Quaternary vegetation and climate of China. In: Wright, H. (Ed.), Global Climates since the Last Glacial Maximum. University of Minnesota Press, Minneapolis, pp. 221–261.
Xiao, J.L., Nakamura, T., Lu, H.Y., Zhang, G.Y., 2002. Holocene climate changes over the desert/loess transition of north-central China. Earth Planet Sc. Lett. 197, 11–18.
Yang, L.H., Wang, T., Zhou, J., Lai, Z.P., Long, H., 2012. OSL chronology and possible forcing mechanisms of dune evolution in the Horqin dunefield in northern China since the Last Glacial Maximum. Quat. Res. 78, 185–196.
Yang, X.P., Scuderi, L.A., 2010. Hydrological and climatic changes in deserts of China since the late Pleistocene. Quat. Res. 73, 1–9.
Yang, X.P., Scuderi, L., Paillou, P., Liu, Z.T., Li, H.W., Ren, X.Z., 2011. Quaternary environmental changes in the drylands of China–a critical review. Quat. Sci. Rev 30, 3219–3233.
Yu, C.X., Luo, Y.L., Sun, X.J., 2008. A high-resolution pollen records from Hani Lake, Jilin, Northeast China showing climate changes between 13.1 cal. Ka B.P and 4.5 cal. Ka B.P. Quat. Sci. 28, 929–938 (in Chinese with English abstract).
Yu, G., Prentice, I.C., Harrison, S.P., Sun, X.J., 1998. Pollen-based biome reconstructions for China at 0 and 6000 years. J. Biogeogr. 25, 1055–1069.
Yu, L.P., Lai, Z.P., 2012. OSL chronology and palaeoclimatic implications of aeolian sediments in the eastern Qaidam Basin of the northeastern Qinghai-Tibetan Plateau. Palaeogeogr. Palaeocl. 337, 120–129.
Yuan, D.X., Cheng, H., Edwards, R.L., Dykoski, C.A., Kelly, M.J., Zhang, M.L., Qing, J.M., Lin, Y.S., Wang, Y.J., Wu, J.Y., Dorale, J.A., An, Z.S., Cai, Y.J., 2004. Timing, duration, and transitions of the Last Interglacial Asian Monsoon. Science 304, 575–578.
Zhang, X.S., 2007. Vegetation map of China and its geographic pattern (Illustration of the vegetation map of the People`s republic of China (1:1000 000). Geology Press, Beijing.
Zhao, X.T., Zhang, J.W., 1984. Basic characteristics of the Holocene sea-level changes along the coast of China. Chin. Quat. Sci. 6, 104–109 (in Chinese).
Zhao, X.T., Han, Y.S., Li, P.R., 1996. Reginal coastal development, sea-level change and their geological records. In: Shi, Y.F., Zhao, X.T. (Eds.), China Sea-level change. Shan dong Science and Technology Press, Jinan, pp. 52–70 (in Chinese).
Zhao, Y., Yu, Z.C., Chen, F.H., 2009a. Spatial and temporal patterns of Holocene vegetation and climate changes in arid and semi-arid China. Quat. Int. 194, 6–18.
Zhao, Y., Yu, Z.C., Chen, F.H., Zhang, J.W., Yang, B., 2009b. Vegetation response to Holocene climate change in monsoon-influenced region of China. Earth-Sci. Rev. 97, 242–256.
Zhao, Y., Yu, Z.C., Zhao, W.W., 2011. Holocene vegetation and climate histories in the eastern Tibetan Plateau: controls by insolation-driven temperature or monsoon-derived precipitation changes? Quat. Sci. Rev. 30, 1173–1184.
Zhu, Z.D., Wu, Z., Liu, S., Di, X., 1980. An outline of Chinese deserts. Science Press, Beijing pp. 107; (in Chinese).